



Investigation of the hydro-mechanical behaviour of GMZ bentonite pellet mixtures

Zhang-Rong Liu¹ · Yu-Jun Cui² · Wei-Min Ye^{1,3} · Bao Chen^{1,3} · Qiong Wang^{1,4} · Yong-Gui Chen^{1,3}

Received: 23 February 2019 / Accepted: 18 April 2020 / Published online: 9 May 2020
© Springer-Verlag GmbH Germany, part of Springer Nature 2020

Abstract

Bentonite pellet mixtures are considered as one of the candidate sealing materials for deep geological disposals of radioactive waste. One of the particularities of this material is the initial heterogeneous distribution of pellets and porosity within the mixture, leading to complex hydro-mechanical behaviour. In this paper, the hydro-mechanical properties of GMZ bentonite pellet mixtures were investigated in the laboratory by carrying out water retention tests on pellet mixtures under constant-volume condition and single pellets under free swelling condition, as well as a infiltration test on a column specimen of pellet mixture. In the infiltration test, the relative humidity and radial swelling pressure were monitored at five heights, the axial swelling pressure was also recorded. The instantaneous profile method was applied to determine the unsaturated hydraulic conductivities. Results show that, in high suction range (> 10 MPa) the water retention curve of pellet mixture under constant-volume condition was comparable to that of a single pellet under free swelling condition, while in low suction range (< 10 MPa) the latter exhibits a much higher water retention capacity. Due to clogging of large pores, the unsaturated hydraulic conductivity decreases as suction decreases to around 25 MPa. However, with further suction decrease, the hydraulic conductivity increases continuously until the value at saturated state, as in the case of most unsaturated soils. The radial swelling pressure at different heights develops with local sudden increase and decrease, which was attributed to local rearrangement of pellets upon wetting. By contrast, as the axial swelling pressure was measured on the global surface of the specimen, it develops in a more regular fashion.

Keywords Bentonite pellets · Hydraulic conductivity · Instantaneous profile method · Relative humidity · Swelling pressure · Water retention

1 Introduction

Granular mixtures of high-density bentonite pellets are considered as one of the candidate sealing materials for deep underground repository of high-level radioactive waste (HLW), where any openings (deposition galleries, access galleries and shafts, etc.) created during the construction of the repository should be effectively sealed to prevent potential preferential pathways for water, gas and radionuclide migration. In addition to its low permeability, high swelling capacity and high radionuclide migration retardation properties, this material has also obvious operational advantages: the pellets can be easily manufactured and emplaced [20, 21].

The use of pellets was proposed decades ago [25, 31] and the feasibility was examined through several field and laboratory tests, such as the RESEAL experiment [14, 29],

✉ Wei-Min Ye
ye_tju@tongji.edu.cn

¹ Department of Geotechnical Engineering, College of Civil Engineering, Tongji University, 1239 Siping Road, Shanghai 200092, China

² Laboratoire Navier/CERMES, Ecole des Ponts ParisTech, Paris, France

³ Key Laboratory of Geotechnical and Underground Engineering of Ministry of Education, Tongji University, Shanghai 200092, China

⁴ Institute for Advanced Study, Tongji University, Shanghai 200092, China

the prototype repository project test [15], the EB (engineered barrier) experiment [12], the SEALEX (SEALing performance Experiments) project [20, 21], the Chinamock-up test [5] and the shot-clay test [11]. In these tests, pellets and pellet/powder mixtures were used to filling either the narrow gaps between buffer and host rock or the annular space between canister and host rock.

Once emplaced in the gallery, the pellet mixture would be subjected to a re-saturation process due to the infiltration of underground water from the host rock. During this process, pellets within the mixture would be progressively wetted and swell under almost confined conditions to fill the inter-pellet voids, decreasing the rate of further water infiltration. Owing to the strong initial heterogeneous porosity [12, 13, 20], the hydro-mechanical behaviour of such material could be much different from that of conventional compacted bentonite blocks. Considering the significant roles of this material in ensuring the overall repository safety, it is essential to understand its hydro-mechanical behaviour.

van Geet et al. [29] studied the hydration process of a column specimen of 50/50 pellet/powder FoCa bentonite mixture by X-ray-computed tomography and showed the progressive decrease in the density of pellets and the apparent homogenization after saturation. Imbert and Villar [14] conducted a series of infiltration tests on 50/50 pellet/powder FoCa bentonite compacted at different dry densities and dimensions and identified a common pattern of swelling pressure development: the swelling pressure increases sharply, then decreases slightly and finally increases again to reach a steady final value. The swelling pressure was found comparable to that of bentonite blocks with the same dry density. Hoffmann et al. [13] investigated the hydro-mechanical response of FEBEX bentonite pellet mixtures and reported that the saturated permeability and the swelling pressure are mainly controlled by the overall dry density rather than the initial grain size distribution. Karnland et al. [16] measured the swelling pressure and saturated hydraulic conductivity of pellets and 70/30 pellet/sand mixtures of MX-80 bentonite using 0.2 M NaCl solution. The results indicated that as the dry density increases, the final swelling pressure increases exponentially while the saturated hydraulic conductivity decreases exponentially. For the pellet mixtures, most of the previous studies were focused on the axial swelling pressure and saturated hydraulic conductivity. Few investigations have been carried out on the radial swelling pressure and the unsaturated hydraulic conductivity [21].

In this study, the hydro-mechanical behaviour of GMZ bentonite pellet mixtures were investigated through water retention tests and an infiltration test on column specimen. The water retention tests involved both the pellet mixture under constant-volume condition and a single pellet under

free swelling condition. In the infiltration test, the evolutions of relative humidity and radial swelling pressure with time at different heights of the specimen as well as the evolution of axial swelling pressure with time were monitored. The instantaneous profile method was applied to determine the unsaturated hydraulic conductivity of the mixture. The results obtained allowed the particular hydro-mechanical behaviour of pellet mixture to be clarified.

2 Materials and methods

2.1 Materials

GMZ bentonite was used in this study. It was extracted from Inner Mongolia autonomous region of China. Some of its basic properties are listed in Table 1 [38]. It is a montmorillonite-dominant soil with high plasticity index (239%), high adsorption capacity ($SSA = 570 \text{ m}^2 \text{ g}^{-1}$) and high cation exchange capacity (77.30 meq/100 g).

The pellets of different sizes were prepared from GMZ bentonite powder as follows: first, bentonite blocks at a target dry density of 1.95 Mg/m^3 were fabricated by statically compacting GMZ bentonite powder in a rigid stainless steel cylindrical cell (50 mm in diameter). During compaction, the axial displacement was monitored to produce a target block height of 30 mm. Then, the compacted block was extruded from the cell and crushed using a jaw crusher, which has five gears holding different maximum gaps between the two jaw plates, producing pellets of different sizes. Finally, the crushed pellets were sieved into seven size classes with particle sizes of 7–5 mm, 5–2 mm, 2–0.9 mm, 0.9–0.5 mm, 0.5–0.25 mm, 0.25–0.075 mm and $< 0.075 \text{ mm}$, respectively. For

Table 1 Basic properties of GMZ bentonite [38]

Property	Description
Main minerals	Montmorillonite (75.4%) Quartz (11.7%) Cristobalite (7.3%) Feldspar (4.3%)
Specific gravity of solid	2.66
Liquid limit/(%)	276
Plastic limit/(%)	37
Total specific surface area (SSA)/ ($\text{m}^2 \text{ g}^{-1}$)	570
Cation exchange capacity/(meq/100 g)	77.30
Main exchanged cation/(meq/100 g)	Na^+ (43.36), $1/2 \text{ Ca}^{2+}$ (29.14) $1/2 \text{ Mg}^{2+}$ (12.33), K^+ (2.51)

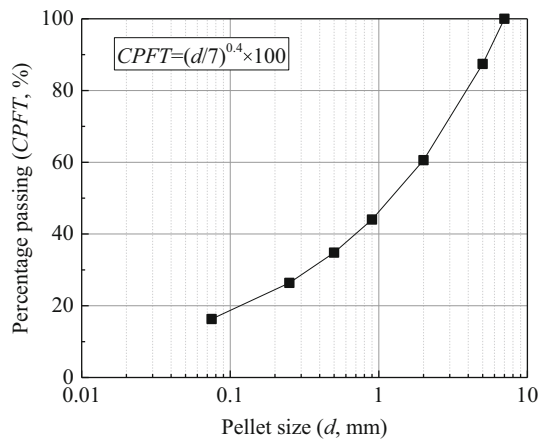


Fig. 1 Pellet size distribution

convenience, they were denoted hereafter by P7, P5, P2, P0.9, P0.5, P0.25 and P0.075, respectively. The classes with pellets size larger than 2.0 mm were regarded as coarse classes (P7 and P5), whereas the others were regarded as fine classes (P2, P0.9, P0.5, P0.25 and P0.075). They were individually stored in seven hermetic plastic boxes in the laboratory at a constant temperature of 20 °C.

Specimens for both water retention and infiltration tests were prepared by assembling pellets with the global pellet size distribution (Fig. 1) obeying to the Andreasen equation [2]:

$$CPFT = (d/7)^{0.4} \times 100 \quad (1)$$

where CPFT denotes the cumulative percentage of pellets finer than diameter d (mm). This pellet size distribution was adopted because it allows the densest packing dry density around 1.45 Mg/m³ under vibration condition in the laboratory [18, 39]. With a target dry density of 1.45 Mg/m³, according to the specimen sizes used in water retention tests (Sect. 2.2) and infiltration test (Sect. 2.3), pellets from each of the seven size classes were weighed at

an accuracy of 0.01 g to their target mass. Then, the coarse pellets (P7 and P5) and fine pellets (P2, P0.9, P0.5, P0.25 and P0.075) were blended evenly in two trays, respectively. The resultant coarse and fine mixtures were equally divided into 3 parts when used in water retention tests or 12 parts when used in infiltration test, respectively. Afterwards, they were introduced into a cylindrical cell through a layer-wise feeding method: the coarse sub-parts and fine sub-parts were independently and alternately fed into the cell, i.e., one layer of coarse sub-parts followed by one layer of fine sub-parts. Finally, the cell together with the mixture in it was vibrated for 180 s on a vibratory table which was cam-driven and could vibrate vertically at a fixed frequency of 50 Hz with an amplitude of 0.3–0.6 mm. The global dry density of the as-vibrated specimen was measured to be around 1.45 Mg/m³, which could be repeatedly achieved through the above-mentioned sampling protocol. It is worth noting that though the adopted feeding method produced initially a sandwich-structured specimen, a relatively homogeneous mixture could be obtained after the operation of vibration.

2.2 Water retention test

The water retention curve of pellet mixtures under constant-volume condition was determined by controlling the suction using both vapour equilibrium technique and osmotic technique. Details of the two techniques can be found in Delage et al. [8], Blatz et al. [4] and Delage and Cui [9]. The vapour equilibrium technique was applied for high suctions ($s \geq 4.2$ MPa) using a setup shown in Fig. 2. The specimen in 50 mm diameter and 35 mm height was constrained in a rigid stainless steel cell with the upper and lower lids tightened by bolts. Vapour of different saturated salt solutions (Table 2) was circulated around the specimen using an air pump. The mass of the specimen was regularly determined at an accuracy of 0.01 g. The equilibrium state

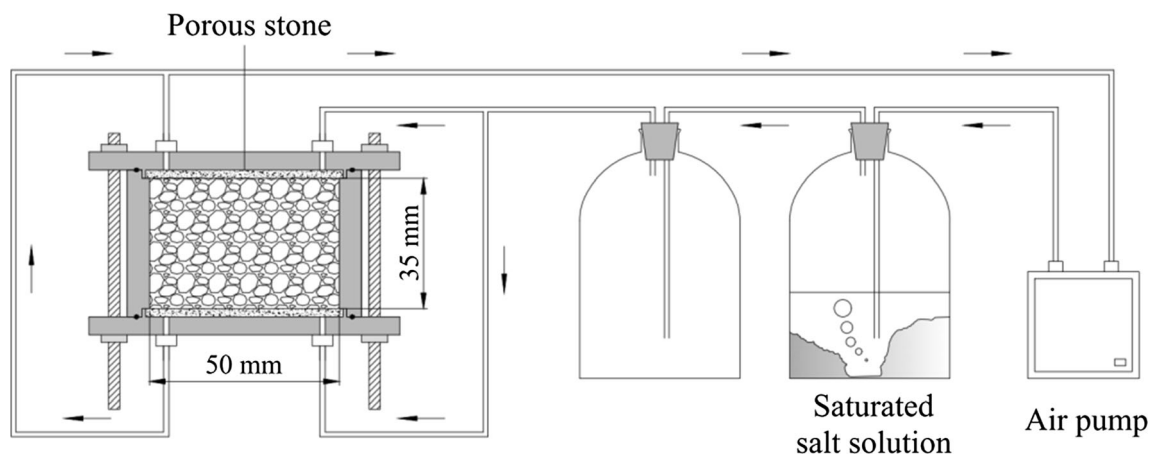


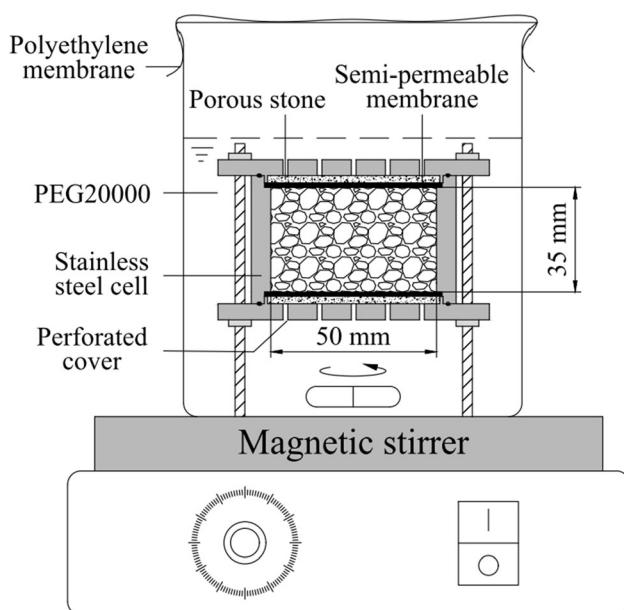
Fig. 2 Experimental setup for suction control using vapour equilibrium technique

Table 2 Saturated salt solutions and corresponding suction at 20 °C [28]

Salt solution	Suction (MPa)
LiCl	309.0
MgCl ₂	150.0
NaBr	70.9
NaCl	38.0
ZnSO ₄	12.6
K ₂ SO ₄	4.2

was considered as reached when no further mass variation was observed (i.e., less than 0.01 g/d). The specimen was then divided into three parts along its height (upper, middle and lower parts). The gravimetric water contents of each part were determined by oven drying them at 105 °C for 24 h and the average value was taken as the equilibrium gravimetric water content of the specimen.

The osmotic technique was applied for low suctions ($s < 4.2$ MPa) using the setup shown in Fig. 3. The specimen in 50 mm diameter and 35 mm height was constrained in a stainless steel constant-volume cell with two perforated covers joined by bolts. A semipermeable membrane was placed between the porous stone (embedded in the perforated cover) and the specimen at each side. The cell was then immersed in a PEG 20,000 (polyethylene glycol) solution which was continuously stirred by a magnetic stirrer for the homogeneity purpose. Several drops of penicillin were added into the solution to prevent from bacteria attack. The solution container was

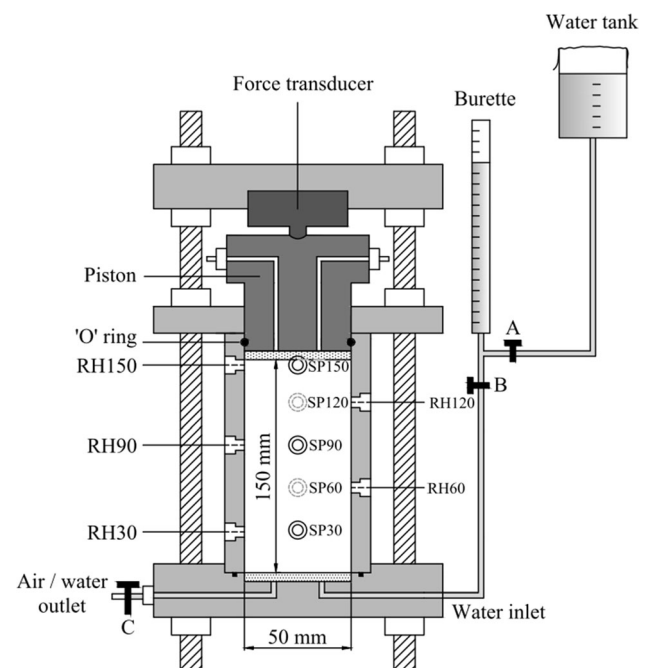
**Fig. 3** Experimental setup for suction control using osmotic technique

covered by a piece of polyethylene membrane for minimizing water evaporation. After 40 days (this time was proved to be enough for suction equilibrium by pre-test), the test was stopped and the specimen was extruded out from the cell. The gravimetric water content of the specimen was determined following a procedure mentioned previously when applying the vapour equilibrium technique. Four PEG 20 000 solutions at initial concentrations of 20.85%, 15.82%, 7.83%, 5.69%, 2.63% corresponding, respectively, to matric suctions of 1.0 MPa, 0.5 MPa, 0.1 MPa, 0.05 MPa and 0.01 MPa were used in this study.

In parallel, the water retention curve of a single pellet under free swelling condition was determined. For high suctions ($s \geq 4.2$ MPa), a handful of pellets contained on a plate were subjected to vapour equilibrium with saturated salt solutions (Table 2) in a desiccator. For low suctions (1.0 MPa and 0.1 MPa), a single pellet was clothed by a semipermeable membrane and immersed in the PEG 20,000 solutions at initial concentrations of 20.85% and 7.83%, respectively. At equilibrium, the water content was determined by oven-drying method and the volume was obtained by hydrostatic weighing the waxed pellet [33]. Accordingly, the dry density was determined.

2.3 Infiltration test

The experimental setup shown in Fig. 4 was used for the infiltration test. The pellet mixtures with the designed pellet size distribution (Fig. 1) were introduced into a rigid stainless steel cell, which has an internal diameter of

**Fig. 4** Schematic view of infiltration setup

50 mm. The resulting specimen had a height of 150 mm and global dry density of 1.45 Mg/m^3 . A piston, a force transducer and an upper lid were attached and fixed on the top side of the specimen to measure the axial swelling pressure. The piston was equipped with an air-discharge channel which was connected to water through a tube. This air-outlet setup allowed the pore air in the specimen to be discharged through water and isolated the specimen from the atmosphere, avoiding thus humidity reduction due to evaporation. Five relative humidity (RH) sensors and five swelling pressure (SP) sensors were installed every 30 mm along the specimen (30, 60, 90, 120 and 150 from the wetting end) through the ports in the wall of the cell. With these sensors, the evolutions of relative humidity and radial swelling pressure at different positions of the specimen were monitored. Water was supplied to the pedestal of the device from a burette, in which the height of water surface was maintained to be about 1.0 m higher than the specimen's bottom side. In other words, the specimen was wetted from its bottom side by water at a pressure of about 10 kPa, which can be ignored in further analysis considering the high suction of the soil specimen. The volume of water intake was regularly recorded through the graduated burette. At the end of the test, the specimen was extracted out from the cell and divided into small discs with thickness of 10 mm for determination of water content and dry density profiles.

3 Experimental results

3.1 Water retention curve

The water retention curves of pellet mixture under constant-volume condition and a single pellet under free swelling condition are presented in Fig. 5 in terms of gravimetric water content versus suction. It appears that when suction is higher than 10 MPa, the pellet mixture under constant-volume condition and a single pellet under free swelling condition have comparable water retention properties. However, when suction is lower than 10 MPa, the single pellet has higher water retention capacity than the pellet mixture. This phenomenon suggests that at high suctions ($> 10 \text{ MPa}$), the water retention curve is independent of initial conditions (initial dry density and fabric, etc.), while it becomes dependent at lower suctions ($< 10 \text{ MPa}$). This observation is consistent with the results reported by Molinero-Guerra [23] on pellet/powder mixture and a single pellet of MX80 bentonite. Similar phenomena were also reported by Villar and Lloret [30] on compacted FEBEX bentonite, Hoffmann et al. [13] and Alonso et al. [1] on FEBEX bentonite pellets, Villar and

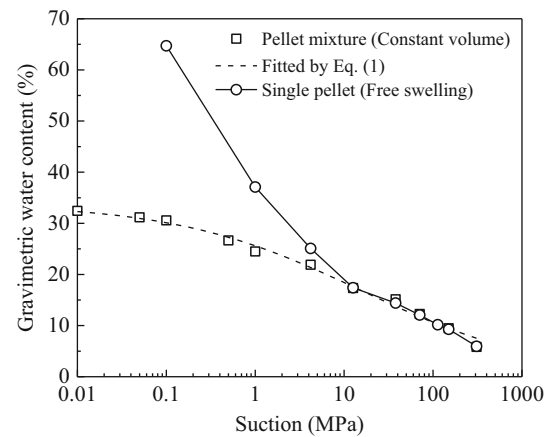


Fig. 5 Water retention curves of pellet mixture under constant-volume condition and a single pellet under free swelling condition

Lloret [30] and Seiphoori et al. [26] on MX-80 bentonite, as well as Wan et al. [32] on GMZ bentonite.

For the pellet mixture, the relationship between water content (w) and suction (s) can be described by the following expression:

$$w = w_{\text{sat}} / [1 + (s/a)^m]^n \quad (2)$$

where w_{sat} stands for water content at saturation ($s = 0$); a , m and n are parameters related to the shape of the curve. As shown in Fig. 5, the measured data can be well fitted by Eq. (2), with parameters $w_{\text{sat}} = 33.8\%$, $a = 15.31 \text{ MPa}$, $m = 0.42$ and $n = 1$.

The dry density of a single pellet versus suction under free swelling condition is replotted in a semi-logarithmic plane in Fig. 6. A good linear relationship was obtained, i.e., the dry density decreased linearly with the decrease in $\lg(s)$. It can be deduced from the fitting line that a dry density of 1.45 Mg/m^3 , which is equal to the global dry density of the pellet mixture under constant-volume condition, will be obtained at a suction of 3.25 MPa. In

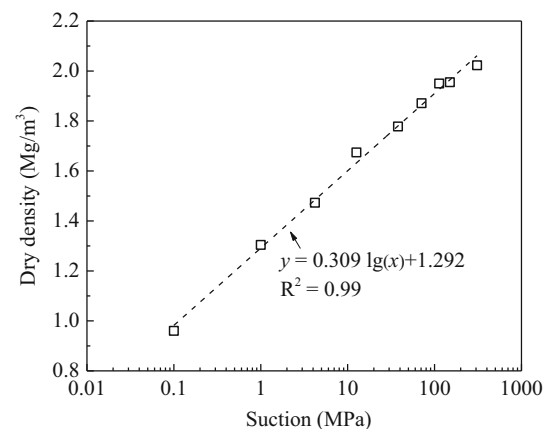


Fig. 6 Evolutions of dry density with respect to suction for a single pellet under free swelling condition

addition, it was observed that subjecting the pellet to vapour equilibrium with suction as low as 4.2 MPa, fissures began to develop. As the suction decreased to 1.0 MPa and 0.1 MPa, both the fissure size and quantity increased. It seems that the development of fissures did not affect the linearity identified.

3.2 Infiltration results

The evolution of relative humidity profiles from the infiltration test is plotted in Fig. 7. As expected, the relative humidity at RH30 increased rapidly and reached 90% after 312 h, then increased gradually to 97.54% after 4560 h. The relative humidity at RH 60 started to increase within 24 h after the infiltration started and reached 90% after 2040 h. The relative humidity at RH90, RH120 and RH150 increased within the first 120 h and reached 90% after 3000 h, 4080 h and 4560 h, respectively. It appears that the increasing rate of RH decreased with the distance from the wetting end.

The values of relative humidity were then converted into total suctions according to the Kelvin’s law:

$$s = -(\rho_w RT/M_w) \ln(RH/100) \tag{3}$$

where ρ_w is the water unit mass (taken equal to 1.0 Mg/m³); R is the universal gas constant (8.31432 J/mol/K); T is the absolute temperature (taken equal to 293.75 K); M_w is molecular mass of water vapour (18.016 kg/kmol).

The suction profiles every 240 h are shown in Fig. 8. At the initial state ($t = 0$), the suction distribution within the specimen was quite homogeneous with a mean value around 102 MPa. After the infiltration started, it was supposed that the suction at the wetting end decreased instantaneously to zero. Then, the suction at different heights decreased progressively at different rates. After 1200 h hydration, the suction profile turned into a nearly straight line with a steep slope in the h - s plane. Afterwards,

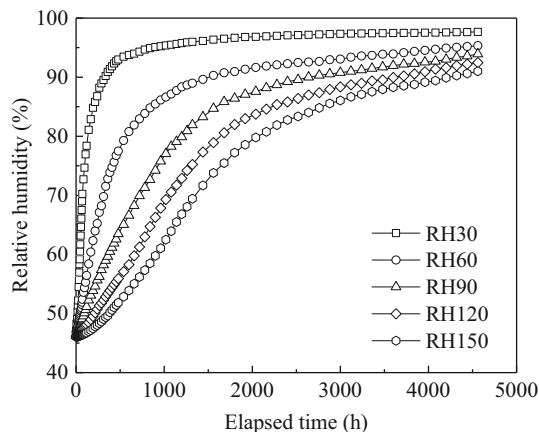


Fig. 7 Evolution of relative humidity during water infiltration

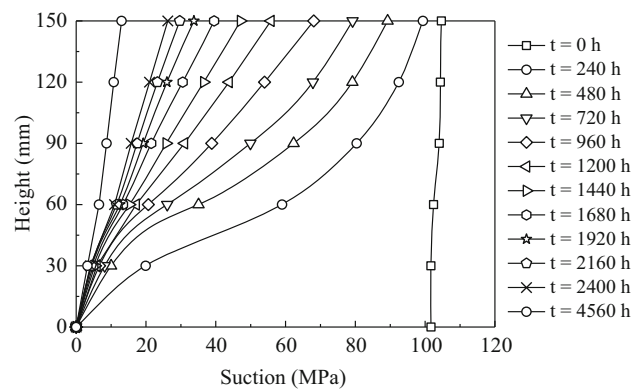


Fig. 8 Suction profiles every 240 h

the slope of the suction profile increased with the infiltration time. At the end of the test ($t = 4560$ h), the suction profile approached a vertical line.

Based on the results of water retention curve [Fig. 5 and Eq. (2)] and suction profiles [Fig. 8 and Eq. (3)], the unsaturated hydraulic conductivity was calculated following the instantaneous profile method as detailed by Cui et al. [6], Ye et al. [37], Wang et al. [34] and Niu et al. [24]. Firstly, the water content profiles were determined using the suction profiles (Fig. 8) with Eq. (2), allowing the water flux (Q) during the times t and $t + dt$ to be calculated. Secondly, the t -time hydraulic gradient (i_t) at the height h was determined with the corresponding slope of suction profile (calculated from Fig. 8):

$$i_t = \frac{ds/dh}{\rho_w g} \tag{4}$$

where ds/dh is the slope of suction profile at the height h , ρ_w is the water unit mass, g is the gravity. Here the suction is considered as the unique driving force of water movement, because of the low water infiltration pressure (10 kPa), low water permeability ($K_{sat} = 9.39 \times 10^{-13}$ m/s) and high suctions (several to hundreds of MPa with low water content, see Fig. 5) of the specimen.

Finally, the unsaturated hydraulic conductivity was calculated based on the generalized Darcy’s law:

$$K = \frac{2Q}{A(i_t + i_{t+dt})} \tag{5}$$

where A is the cross section of the specimen.

The calculated unsaturated hydraulic conductivity is plotted versus suction in Fig. 9, where the saturated hydraulic conductivity (9.39×10^{-13} m/s) was determined on a specimen with the same dry density (1.45 Mg/m³) and diameter (50 mm) but smaller height (35 mm) under constant-volume condition by 1000 kPa water pressure. It can be observed that as suction decreases, the hydraulic conductivity at different heights of the specimen evolves

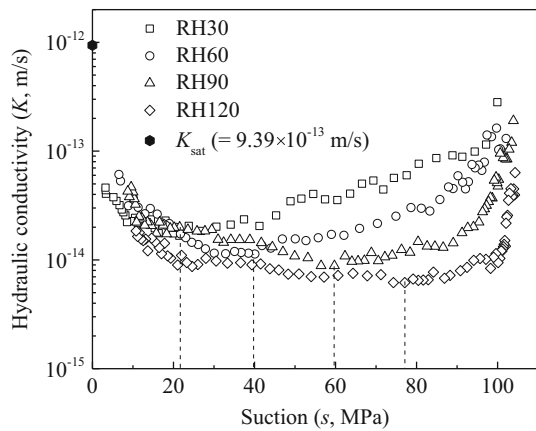


Fig. 9 Hydraulic conductivity versus suction for different measurement heights

following different paths but a similar trend: a decrease followed by an increase. The suction corresponding to the minimum unsaturated hydraulic conductivity increases with the increase in the measurement height. For a suction larger than 40 MPa, the higher the measuring height, the smaller the unsaturated hydraulic conductivity. As suction decreases from 40 to 15 MPa, the hydraulic conductivity at $h = 30, 90, 120$ mm remain nearly constant while that at $h = 60$ mm increases slightly. As suction further decreases to lower value, the hydraulic conductivity increases in a comparable trend and tends to head for the value of saturated hydraulic conductivity ($K_{sat} = 9.39 \times 10^{-13}$ m/s).

The evolutions of axial and radial swelling pressures with infiltration time are shown in Fig. 10. It can be seen that the swelling pressure at different heights also evolved in different trends. As the infiltration test started, the radial swelling pressure at SP30 increased rapidly to a peak value of 1.15 MPa at $t = 840$ h, then decreased to a value of 1.03 MPa at $t = 1608$ h. Successively, the swelling pressure increased slightly to a second peak value of 1.08 MPa at $t = 3360$ h before it decreased gradually to a lower

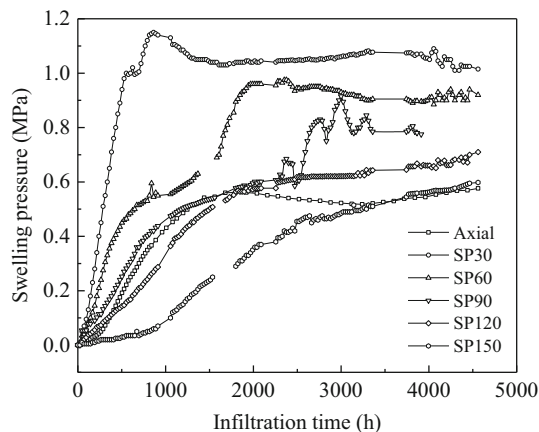
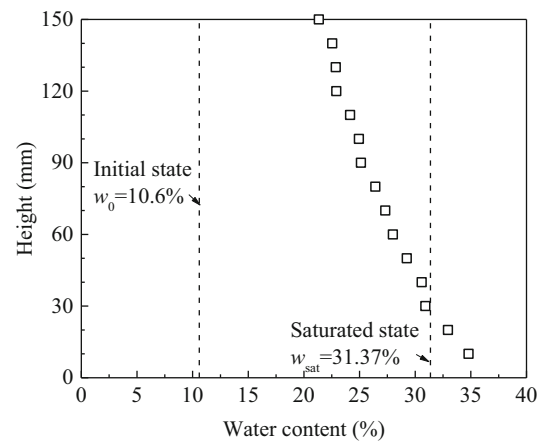


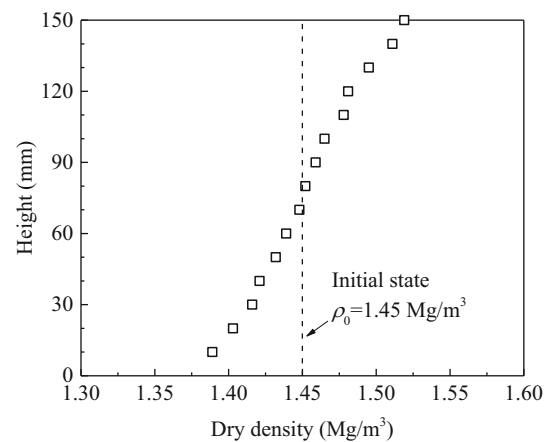
Fig. 10 Evolutions of axial and radial swelling pressures

value. The swelling pressure at SP60 increased quickly to a first peak of 0.55 MPa within the first 840 h. After a short plateau, it increased again until reaching a second peak of 0.98 MPa at $t = 2328$ h, after which it decreased slightly to a steady value of about 0.9 MPa after $t = 3240$ h. The swelling pressure measured at SP90 developed in a similar fashion as that at SP60; but at SP90 the curve after the first peak exhibited much more fluctuation. At a lower rate, the swelling pressure at SP120 and SP150 increased continuously to a value of 0.71 MPa and 0.60 MPa at the end of the test, respectively. The final swelling pressure at lower height has a higher value. For the axial swelling pressure, it evolved in a smoother trend: increased first to a peak value of 0.56 MPa at $t = 1800$ h and then decreased to a lower value of 0.52 MPa at $t = 3240$ h before a new increasing.

At the end of the infiltration test, the water content and dry density were determined for the positions every 10 mm along the height of the specimen. The results are shown in Fig. 11a, b, respectively. As expected, the water content decreased while the dry density increased as the height



(a) Water content distribution



(b) Dry density distribution

Fig. 11 Water content and dry density distributions at the end of the infiltration test

increased. In the zone near the wetting end ($h = 0\text{--}60\text{ mm}$), the dry density was found to be $1.39\text{--}1.44\text{ Mg/m}^3$, lower than the initial value (1.45 Mg/m^3), while in the upper zone ($h = 60\text{--}150\text{ mm}$), higher dry densities ($1.45\text{--}1.52\text{ Mg/m}^3$) were observed. This must result from the swelling of the lower part and the compaction of the upper part of the specimen [3].

The degree of saturation (S_r) at different heights was calculated using the measured water contents and dry densities (Fig. 11). Results show that the zone near the wetting end ($h < 10\text{ mm}$) was already saturated by water ($S_r = 1.01$), while the other area ($h > 10\text{ mm}$) was still in unsaturated state ($S_r < 1.0$). The value of degree of saturation slightly higher than 1.0 may be due to: (1) possible experimental error resulting from the inflow of water from the bottom during slicing the dismantled specimen and (2) the average density of adsorbed water which could be higher than 1.0 Mg/m^3 [30]. It seems that the re-saturation process of the specimen should last a long period of time.

4 Discussion

The comparable water retention curves of pellet mixture and a single pellet at high suctions ($> 10\text{ MPa}$, Fig. 5) suggests the independence of water retention behaviour with respect to the initial conditions (dry density and fabric, etc.) and confining condition. This is because in high suction range ($> 10\text{ MPa}$), water is essentially adsorbed by clay minerals or inside the pellets. Thus, no difference exists between pellet mixture and single pellet and the confining condition has no effect because the presence of macro-pores between the pellets in the mixture. By contrast, in low suction range ($< 10\text{ MPa}$), under confined condition, as the total amount of inter-pellet pores is limited, the water content increase is slowed down when these pores are fully filled by swollen clay particles. On the contrary, under free swelling condition for the single pellet, this limitation related to the inter-pellet pores does not exist. Thus, more water is allowed by larger pellet swelling. Predictably, given unconfined condition, higher water retention capacity of the pellet mixture is expected.

Figure 9 indicates that as suction decreased from a high value to zero, the hydraulic conductivities at different heights first decreased and then increased. This result was different from the observation commonly made on non-expansive unsaturated soils, for which the hydraulic conductivity increases in a continuous way upon wetting as a result of the increase in degree of saturation [7]. As pointed out by Cui et al. [6], Ye et al. [37], Wang et al. [34] and Niu et al. [24], water transfer in compacted bentonite or bentonite-based materials is primarily governed by the network of large pores. Upon wetting, the initial decrease

in hydraulic conductivity is caused by the progressive clogging of large pores due to the gel creation from bentonite aggregate hydration and exfoliation; the subsequent increase in hydraulic conductivity is attributed to the decrease in water retention energy defined by the suction.

Figure 9 also indicates that at given suctions (s), the unsaturated hydraulic conductivity (K) at different heights were not comparable. Cui et al. [6] and Wang et al. [34] also reported different K - s relationships at different heights of column specimen of bentonite/sand mixtures. They attributed this phenomenon to the effect of critical gradient: water flow with hydraulic gradient lower than the critical gradient is of non-Darcian flow nature and should be excluded in the determination of K - s relationship. Following this idea, the water fluxes (q) versus hydraulic gradient (i) for each suction level obtained from this study are plotted in Fig. 12. It appears that for a given suction, the relationship between water flux and hydraulic gradient is bilinear with two slopes: the slope at high gradients is larger than that at low gradients. This can be explained by the high activation energy of the water adsorbed on the clay particles, which increases with the decreasing distance to the surface of the clay particles [35]. When the hydraulic gradient is not large enough to overcome the activation energy, the adsorbed water behaves as “immobile film” without contribution to water flow and thus the water fluxes are small (Fig. 12). As the hydraulic gradient increases, this energy is overcome locally and the adsorbed water can be displaced, resulting in larger water fluxes (Fig. 12). Clearly, for each suction value, there is a “critical gradient” below which the water flow is of non-Darcian nature and should not be considered when calculating the hydraulic conductivity [10].

Considering the critical gradient effect, the hydraulic conductivity was corrected by considering water flow only at high hydraulic gradients. This correction led to a unique K - s relationship independent of the measurement height (Fig. 13). It can be observed that K decreased from

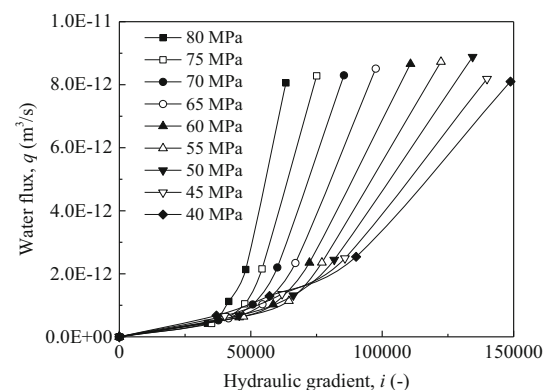


Fig. 12 Water fluxes versus hydraulic gradient for different suctions

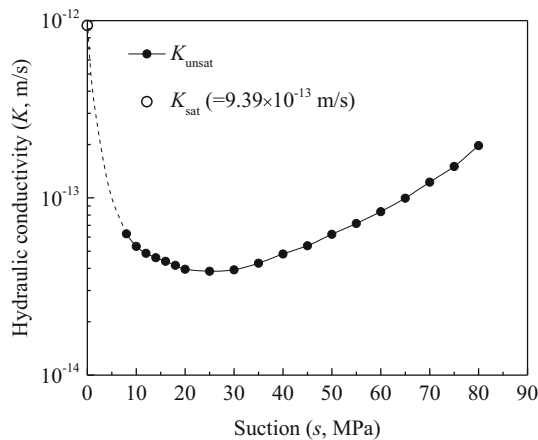


Fig. 13 Hydraulic conductivity versus suction

1.97×10^{-13} to 3.85×10^{-14} m/s when suction decreased from 80 to 25 MPa. As suction further decreased to 8 MPa, K slightly increased to 6.27×10^{-14} m/s with a tendency to the saturated hydraulic conductivity (9.39×10^{-13} m/s).

The difference among the evolution curves of radial swelling pressure at different heights (Fig. 10) could be related to the local swelling, collapse and displacement of pellets upon wetting. During hydration, water tended to flow preferentially into the inter-pellet voids because their sizes are much larger than those inside the pellets. Simultaneously, parts of the inter-pellet water will be adsorbed by the pellets, leading to swelling of the pellets and thus filling of the inter-pellet pores. However, due to the limited inter-pellet pore space, the adjacent swelling pellets will compress each other, resulting in the collapse of pellets. This collapse may also be induced by the increasing vertical swelling pressure. In addition, the initial position of local pellets may also be changed due to the mechanical interactions between them. The displacement of local pellets will cause sudden increase or decrease in radial swelling pressure. Therefore, it was observed that the radial swelling pressures at heights of 30 mm, 60 mm and 90 mm first increased rapidly and then decrease slightly (Fig. 10). The fluctuation on the curves indicates the complicated competition between the swelling and collapse of pellets. At height of 90 mm, the sudden increase followed by a decrease in radial swelling pressure between $t = 2300$ h and $t = 3800$ h indicates the drastic swelling and collapse of the local pellets. The continuously increasing radial swelling pressure at height of 120 mm and 150 mm suggests a dynamic equilibrium between swelling and collapse of the local pellets.

The swelling and collapse of local pellets during hydration can also be identified from the evolution curves of radial swelling pressure with suction (Fig. 14). For sensor SP30, the swelling pressure increased slowly as suction decreased from 102 to 40 MPa. Then, it increased

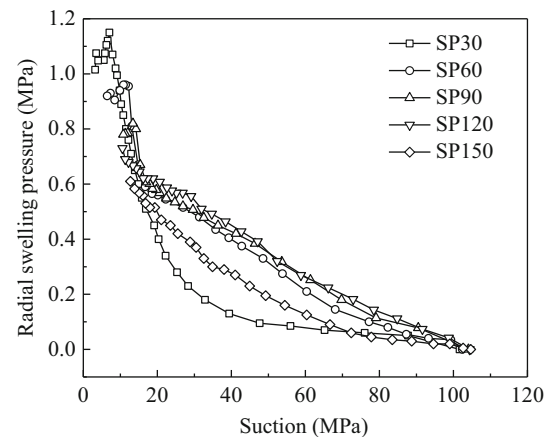


Fig. 14 Radial swelling pressure versus suction at different heights

rapidly to a peak value at a suction of 7.5 MPa before turning into a slight decrease. The swelling pressure at sensors SP60, SP90 and SP120 increased in comparable trends as suction decreased from the initial state to a value of around 16 MPa. As suction further decreased, the swelling pressure at sensors SP60 and SP90 increased sharply to peak values at a suction of 13.5 MPa before decreasing slightly, while the swelling pressure at sensor SP120 increased continuously. Further examination shows that the swelling pressure at sensor SP150 grew at a lower rate than those at sensors SP60, SP90 and SP120. As swelling pressure is governed by both suction and dry density, this phenomenon suggests a heterogeneous distribution of the local dry density within the specimen: the local dry densities at sensors SP30 and SP150 were lower than those at sensors SP60, SP90 and SP120. Actually, due to the particle segregation after vibration, more fine pellets on the lower part (near to SP30) and more large pellets on the upper part (near to SP150) of the initial prepared specimen were observed, leading to a less dense soil structure [19]. During infiltration, the specimen would undergo a complicated structure homogenization process: on the one hand, the initial heterogeneity tended to be reduced due to swelling of pellets and filling of inter-pellet pores, on the other hand additional heterogeneity could be caused by the friction between the pellets and the lateral wall as well as the diverse compressibility of pellets at different saturation states. However, because of the extremely low rate of water migration, this homogenization process was not completed even at the end of the test (Fig. 11). The comparable swelling pressures at a given suction at sensors SP60, SP90 and SP120 suggest similar dry density at these levels. When suction tended to zero, the sharp increase followed by a decrease in swelling pressures at sensors SP30, SP60 and SP90 suggests the drastic swelling and then collapse of local large pellets.

Unlike the radial swelling pressures, the axial swelling pressure evolved following a smoother path, without sudden increase and decrease (Fig. 10). This is because the axial swelling pressure was measured at the top surface by a force transducer; thus, it depends on the global dry density of the specimen. In other words, the evolution of axial swelling pressure reflected the competition between the swelling and collapse of all pellets within the specimen. The axial swelling pressure increased before a peak value due to the prevailing swelling of pellets and then slightly decreased owing to the dominant collapse of pellets within the specimen. The collapse decreased the inter-pellet macro-pores, leading in turn to the decrease in collapse. Thus, the swelling process became dominant again with the new increasing of axial swelling pressure. According to the relationship between axial swelling pressure and dry density on compacted GMZ bentonite derived by Ye et al. [36], the final axial swelling pressure was estimated at 0.913 MPa when the specimen (1.45 Mg/m^3) gets saturated completely.

Fundamentally, the soil structure plays a significant role in the hydro-mechanical behaviour. For further understanding the hydro-mechanical behaviour of GMZ bentonite pellets, the evolution of the structure of pellet mixture with suction requires further investigation either via MIP, ESEM or μ -CT [22, 27]. In addition, a constitutive model for the hydro-mechanical behaviour is needed for a numerical study on the long-term performance of the bentonite pellet mixtures used in a HLW repository. In this regard, the pioneer work of Alonso et al. [1] and Li et al. [17] could be inspiring.

5 Conclusions

The hydro-mechanical properties of pellet mixture of GMZ bentonite were investigated in the laboratory by carrying out water retention test and infiltration test. Based on the obtained results, the following conclusions can be drawn:

In high suction range ($> 10 \text{ MPa}$), the water retention curve of pellet mixture under constant-volume condition was comparable to that of a single pellet under free swelling condition because water is essentially adsorbed by clay minerals or inside the pellets, while in low suction range ($< 10 \text{ MPa}$), the water retention capacity of pellet mixture was much lower than that of a single pellet due to the limited total amount of inter-pellet pores under constant-volume condition.

The unsaturated hydraulic conductivity of pellet mixture decreased as suction decreased to around 25 MPa and then tended to increase continuously to the value at saturated state ($9.39 \times 10^{-13} \text{ m/s}$) as suction further decreased to zero. The initial decrease in unsaturated hydraulic

conductivity was attributed to the progressive clogging of large pores induced by the gel creation from bentonite aggregate hydration and clay particle exfoliation, while the subsequent increase resulted from the decrease in water retention energy defined by the suction.

Different evolution curves of radial swelling pressure at different heights were observed. It is believed that the initial heterogeneous distribution of local pellet and porosity were responsible for such difference. Some sudden increase and decrease in radial swelling pressure were also observed, which could be induced by the swelling, collapse and displacement of local pellets as suction decreases. By contrast, the axial swelling pressure grew in a more regular fashion because it is the competition between swelling and collapse of pellets.

Acknowledgements The financial supports of the National Nature Science Foundation of China (41527801, 41672271 and 41807237) and the Shanghai Pujiang Program (18PJ1410200) are greatly acknowledged.

References

- Alonso EE, Hoffmann C, Romero E (2011) Hydromechanical behaviour of compacted granular expansive mixtures: experimental and constitutive study. *Géotechnique* 61(4):329–344. <https://doi.org/10.1680/geot.2011.61.4.329>
- Andreasen AHM, Andersen J (1930) Relation between grain size and interstitial space in products of unconsolidated granules. *Kolloid-Zeitschrift* 50:217–228
- Bian X, Cui YJ, Li XZ (2019) Voids effect on the swelling behaviour of compacted bentonite. *Géotechnique* 67(7):593–605. <https://doi.org/10.1680/jgeot.17.p.283>
- Blatz JA, Cui YJ, Oldecop L (2008) Vapour equilibrium and osmotic technique for suction control. *Geotech Geol Eng* 26:661–673. <https://doi.org/10.1007/s10706-008-9196-1>
- Chen L, Liu YM, Wang J, Gao SF, Xie JL, Ma LK, Zhao XG, Li YW, Liu J (2014) Investigation of the thermal-hydro-mechanical (THM) behavior of GMZ bentonite in the China-Mock-up test. *Eng Geol* 172:57–68. <https://doi.org/10.1016/j.enggeo.2014.01.008>
- Cui YJ, Tang AM, Loiseau C, Delage P (2008) Determining the unsaturated hydraulic conductivity of a compacted sand-bentonite mixture under constant-volume and free-swell conditions. *Phys Chem Earth* 33(S1):S462–S471. <https://doi.org/10.1016/j.pce.2008.10.017>
- Daniel DE (1982) Measurement of hydraulic conductivity of unsaturated soils with thermocouple psychrometers. *Soil Sci Soc Am J* 20(6):1125–1129. <https://doi.org/10.2136/sssaj1982.03615995004600060001x>
- Delage P, Howat M, Cui YJ (1998) The relationship between suction and swelling properties in a heavily compacted unsaturated clay. *Eng Geol* 50(1–2):31–48. [https://doi.org/10.1016/S0013-7952\(97\)00083-5](https://doi.org/10.1016/S0013-7952(97)00083-5)
- Delage P, Cui YJ (2008) An evaluation of the osmotic method of controlling suction. *Geomech Geoeng* 3(1):1–11. <https://doi.org/10.1080/17486020701868379>
- Dixon DA, Gray MN, Hnatiw D (1992) Critical gradients and pressures in dense swelling clays. *Can Geotech J* 29(6):1113–1119. <https://doi.org/10.1139/t92-129>

11. Ferrari A, Seiphoori A, Rüedi J, Laloui L (2014) Shot-clay MX-80 bentonite: an assessment of the hydro-mechanical behaviour. *Eng Geol* 173:10–18. <https://doi.org/10.1016/j.enggeo.2014.01.009>
12. García-Siñeriz JL, Villar MV, Rey M, Palacios B (2015) Engineered barrier of bentonite pellets and compacted blocks: state after reaching saturation. *Eng Geol* 192:33–45. <https://doi.org/10.1016/j.enggeo.2015.04.002>
13. Hoffmann C, Alonso EE, Romero E (2007) Hydro-mechanical behaviour of bentonite pellet mixtures. *Phys Chem Earth* 32(8–14):832–849. <https://doi.org/10.1016/j.pce.2006.04.037>
14. Imbert C, Villar MV (2006) Hydro-mechanical response of a bentonite pellets/powder mixture upon infiltration. *Appl Clay Sci* 32(3–4):197–209. <https://doi.org/10.1016/j.clay.2006.01.005>
15. Johannesson LE, Bögesson L, Goudarzi R, Sandén T, Gunnarsson D, Svemar C (2007) Prototype repository: a full scale experiment at Äspö HRL. *Phys Chem Earth* 32:58–76. <https://doi.org/10.1016/j.pce.2006.04.027>
16. Karnland O, Nilsson U, Weber H, Wersin P (2008) Sealing ability of Wyoming bentonite pellets foreseen as buffer material—laboratory results. *Phys Chem Earth* 33:S472–S475. <https://doi.org/10.1016/j.pce.2008.10.024>
17. Li ZZ, Su G, Zheng Q, Nyuyen TS (2019) A dual-porosity model for the study of chemical effects on the swelling behaviour of MX-80 bentonite. *Acta Geotech*. <https://doi.org/10.1007/s11440-019-00762-5> (in press)
18. Liu ZR, Ye WM, Zhang Z, Wang Q, Chen YG, Cui YJ (2019) Particle size ratio and distribution effects on packing behaviour of crushed GMZ bentonite pellets. *Powder Technol* 351:92–101. <https://doi.org/10.1016/j.powtec.2019.03.038>
19. Liu ZR, Cui YJ, Ye WM, Zhang Z, Wang Q, Chen B (2020) Investigation on vibration induced segregation behaviour of crushed GMZ bentonite pellet mixtures. *Constr Build Mater* 241:117949. <https://doi.org/10.1016/j.conbuildmat.2019.117949>
20. Molinero-Guerra A, Mokni N, Delage P, Cui YJ, Tang AM, Aïmedieu P, Bernier F, Bornert M (2017) In-depth characterisation of a mixture composed of powder/pellets MX80 bentonite. *Appl Clay Sci* 135:538–546. <https://doi.org/10.1016/j.clay.2016.10.030>
21. Molinero-Guerra A, Cui YJ, Mokni N, Delage P, Bornert M, Aïmedieu P, Tang AM, Bernier F (2018) Investigation of the hydro-mechanical behaviour of a pellet/powder MX80 bentonite mixture using an infiltration column. *Eng Geol* 243:18–25. <https://doi.org/10.1016/j.enggeo.2018.06.006>
22. Molinero-Guerra A, Aïmedieu P, Bornert M, Cui YJ, Tang AM, Sun Z, Mokni N, Delage P, Bernier F (2018) Analysis of the structural changes of a pellet/powder bentonite mixture upon wetting by X-ray computed microtomography. *Appl Clay Sci* 165:164–169. <https://doi.org/10.1016/j.clay.2018.07.043>
23. Molinero-Guerra A (2018) Experimental and numerical characterizations of the hydro-mechanical behavior of a heterogeneous material: pellet/powder bentonite mixture. University of Paris-Est, Paris
24. Niu WJ, Ye WM, Song X (2019) Unsaturated permeability of Gaomiaozi bentonite under partially free-swelling conditions. *Acta Geotech*. <https://doi.org/10.1007/s11440-019-00788-9> (in press)
25. Salo JP, Kukkola T (1989) Bentonite pellets, an alternative buffer material for spent fuel canister deposition holes. NEA/CEC Workshop “Sealing of Radioactive Waste Repositories”. (Braunschweig, Germany), OECD, Paris
26. Seiphoori A, Ferrari A, Laloui L (2014) Water retention behaviour and microstructural evolution of MX-80 bentonite during wetting and drying cycles. *Géotechnique* 64(9):721–734. <https://doi.org/10.1680/geot.14.P.017>
27. Sun HQ, Mašin D, Najser J, Neděla V, Navrátilová E (2019) Fractal characteristics of pore structure of compacted bentonite studied by ESEM and MIP methods. *Acta Geotech*. <https://doi.org/10.1007/s11440-019-00857-z> (in press)
28. Tang AM, Cui YJ (2005) Controlling suction by the vapour equilibrium technique at different temperatures and its application in determining the water retention properties of MX80 clay. *Can Geotech J* 42:1–10. <https://doi.org/10.1139/T04-082>
29. Van Geet M, Volckaert G, Roels S (2005) The use of microfocus X-ray computed tomography in characterising the hydration of a clay pellet/powder mixture. *Appl Clay Sci* 29(2):73–87. <https://doi.org/10.1016/j.clay.2004.12.007>
30. Villar MV, Lloret A (2004) Influence of temperature on the hydro-mechanical behaviour of a compacted bentonite. *Appl Clay Sci* 26(1–4):337–350. <https://doi.org/10.1016/j.clay.2003.12.026>
31. Volckaert G, Bernier F, Alonso E, Gens A, Samper J, Villar MV, Martín PL, Cuevas J, Campos R, Thomas HR, Imbert C, Zingarelli V (1996) Thermal-hydraulic-mechanical and geochemical behaviour of the clay barrier in radioactive waste repositories (model development and validation). Nuclear Science and Technology. EUR 16744. Commission of the European Communities, Luxembourg. 722 pp
32. Wan M, Ye WM, Chen YG, Cui YJ, Wang J (2015) Influence of temperature on the water retention properties of compacted GMZ01 bentonite. *Environ Earth Sci* 73(8):4053–4061. <https://doi.org/10.1007/s12665-014-3690-y>
33. Wan M, Delage P, Tang AM, Talandier J (2013) Water retention properties of the Callovo-Oxfordian claystone. *Int J Rock Mech Min Sci* 64(12):96–104. <https://doi.org/10.1016/j.ijrmmms.2013.08.020>
34. Wang Q, Cui YJ, Tang AM, Barnichon JD, Saba S, Ye WM (2013) Hydraulic conductivity and microstructure changes of compacted bentonite/sand mixture during hydration. *Eng Geol* 164:67–76. <https://doi.org/10.1016/j.enggeo.2013.06.013>
35. Wang SW, Zhu W, Fei K, Xu CY, Zhang N (2018) Study on non-darcian flow sand-clay mixtures. *Appl Clay Sci* 151:102–108. <https://doi.org/10.1016/j.clay.2017.10.028>
36. Ye WM, Schaze S, Qian LX, Wang J, Arifin Y (2007) Characteristics of swelling pressure of densely compacted gaomiaozi bentonite GMZ01. *Chin J Rock Mech Eng* 26:3861–3865 (in Chinese)
37. Ye WM, Cui YJ, Qian LX, Chen B (2009) An experimental study of the water transfer through confined compacted GMZ bentonite. *Eng Geol* 108(3–4):169–176. <https://doi.org/10.1016/j.enggeo.2009.08.003>
38. Ye WM, Chen YG, Chen B, Wang Q, Wang J (2010) Advances on the knowledge of the buffer/backfill properties of heavily-compacted GMZ bentonite. *Eng Geol* 116(1):12–20. <https://doi.org/10.1016/j.enggeo.2010.06.002>
39. Zhang Z, Ye WM, Liu ZR, Chen BC, Cui YJ (2018) Influences of PSD curve and vibration on the packing dry density of crushed bentonite pellet mixtures. *Constr Build Mater* 185:246–255. <https://doi.org/10.1016/j.conbuildmat.2018.07.096>